Trajectory Planning and Sliding-Mode Velocity Control for an Under-Actuated Hovercraft Vehicle

Lukas Pröhl
Chair of Mechatronics
University of Rostock
Rostock, Germany
Lukas.Proehl@uni-rostock.de

Harald Aschemann
Chair of Mechatronics
University of Rostock
Rostock, Germany
Harald.Aschemann@uni-rostock.de

IECON 2021 - 47th Annual Conference of the IEEE Industrial Electronics Society | 978-1-6654-3554-3/21/$31.00 ©2021 IEEE | DOI: 10.1109/IECON48115.2021.9589350

***Abstract*—This paper presents a sliding-mode approach for the robust tracking control of the body-fixed velocities of an under-actuated hovercraft vehicle. Pontryagin's Maximum Principle is applied for an optimal trajectory planning – providing optimal state and input variables for feedforward control. Moreover, the design-related cross-couplings of the two control inputs are analysed and addressed by a heuristic approach. The performance of the proposed nonlinear control structure is investigated by simulations using an identified model of a corresponding experimental vehicle.**

***Index Terms*—Motion control, under-actuated systems, sliding-mode control, mechatronics**

I. Introduction

The objective of this work is the model-based control of an experimental hovercraft vehicle, which was build at the Chair of Mechatronics, University of Rostock. Due to its non-linear dynamics, its under-actuation as well as imperfections of the used sensor configuration, the hovercraft vehicle represents a challenging control task. The characteristic feature of the hovercraft is given by a pressurized air cushion below the vehicle. This serves for a reduction of the friction between the vehicle and the ground, and it allows for a floating operation of the vehicle. As the hovercraft is designed to have no contact to the ground, thrust propellers are applied to produce an air flow propelling the vehicle. Here, a traction system with two fixed thrusters present a prevalent set up, see e.g. [4] as well as [5]. In this paper, however, the propulsion system involves only one thrust propeller in combination with two tiltable blades to control the air flow. With this propulsion topology it is not possible to apply a rotational torque without generating a traction force in the longitudinal direction. A proper heuristic, considering this interaction of the control inputs, is one objective of this paper.

Utilizing the differential flatness of the presented model, a non-linear control approach for the tracking of the global position coordinates was elaborated in [6]. However, a feedback of the global position coordinates is not foreseen with the given set up and conclusively, the focus is on the control of the local dynamics. As an extension to the flatness-based approach proposed in [7], the given paper presents a non-linear sliding-mode control (SMC, see e.g. [8]) for the velocities of the vehicle. This robust feedback control is combined with feedforward control based on the optimal trajectory planning, evaluated by Pontryagin's Maximum Principle.

For the application of the proposed methods, a mathematical model is derived within Sect. II. It serves for both the simulation of the vehicle motion and control design as well as trajectory planning. The feedforward control design w.r.t. a desired trajectory is elaborated in Sect. III. Sect. IV presents a sliding-mode tracking control for the velocities of the vehicle. The overall control approach is investigated via simulations in Sect. V, and conclusions are given in Sect. VI.

II. Modeling of the system behavior

This section presents the derivation of a mathematical description of the hovercraft vehicle. A general model for the longitudinal and lateral dynamic of the vehicle is discussed in Subsec. II-A, whereas Subsec. II-B addresses the specific actuator characteristic of the set up.

A. Horizontal System Model

The model of the horizontal motion can be derived in analogy to the equations of motion for an under-actuated ship like in [1], [2], or [3]. A summary of the modeling is also given in [7]. For the description of the system behavior with body-fixed velocities, the transformation

$$\underbrace{\begin{bmatrix}\dot{x}\\ \dot{y}\\ \dot{\gamma}\end{bmatrix}}_{\underline{\dot{x}}_w} = \underbrace{\begin{bmatrix}\cos(\gamma) & -\sin(\gamma) & 0\\ \sin(\gamma) & \cos(\gamma) & 0\\ 0 & 0 & 1\end{bmatrix}}_{\underline{T}} \underbrace{\begin{bmatrix}u\\ v\\ r\end{bmatrix}}_{\underline{x}_b}. \tag{1}$$

holds. Here, the body-fixed velocities are described by body-fixed states $\underline{x}_b = [u \quad v \quad r]^T$, whereas the global pose of the vehicle is given in world coordinates $\underline{x}_w = [x \quad y \quad \gamma]^T$.

The mechanical forces and torques acting on the hovercraft vehicle are depicted in Fig. 1. Here, the system parameters m and J represent the mass of the hovercraft as well as the mass moment of inertia corresponding to the orientation angle γ. The damping coefficients d and d_r for the translational and rotatory motions characterize velocity-proportional resistances like friction and air drag. As control inputs, the propelling force F as well as the torque M are considered. Additionally, a disturbance force ΔF is introduced to account for external

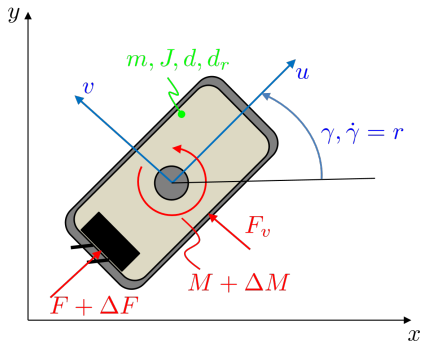

Fig. 1. Mathematical model of horizontal dynamics of the hovercraft vehicle.

disturbances, model uncertainty as well as uncertainties of the actuator characteristics. The disturbance torque ΔM mainly addresses an additional torque caused by the uplift impeller. The disturbance force in transverse direction F_v is considered as small and will be neglected in the sequel.

The control design, however, will be based on the equations of motion within the body-fixed uv-coordinate system of the hovercraft vehicle.

$$\underbrace{\begin{bmatrix}\dot{u}\\ \dot{v}\\ \dot{r}\end{bmatrix}}_{\dot{\underline{x}}_b} = \underbrace{\begin{bmatrix}-\frac{d}{m}u+v\cdot r\\ -\frac{d}{m}v-u\cdot r\\ -\frac{d_r}{J}r\end{bmatrix}}_{\underline{a}(\underline{x}_b)} + \underbrace{\begin{bmatrix}\frac{1}{m} & 0\\ 0 & 0\\ 0 & \frac{1}{J}\end{bmatrix}}_{\underline{B}} \cdot \underbrace{\begin{bmatrix}F\\ M\end{bmatrix}}_{\underline{u}} + \underbrace{\begin{bmatrix}\frac{1}{m} & 0\\ 0 & 0\\ 0 & \frac{1}{J}\end{bmatrix}}_{\underline{E}} \cdot \underbrace{\begin{bmatrix}\Delta F\\ \Delta M\end{bmatrix}}_{\underline{z}} . \tag{2}$$

B. Actuator Characteristic of the Control Inputs

Based on the geometrical setup of the propulsion system, the propulsion force $F(t)$ in longitudinal direction as well as the torque $M(t)$ depend on

- the rotational speed n_p of the propulsion propeller producing the total thrust S,
- the tilt angle μ of the air blades.

In Fig. 2, the actuator characteristics of the force $F = \phi_F(S,\mu)$ as well as of the torque $M = \phi_M(S,\mu)$ are presented. Here, the geometrical structure of the hovercraft vehicle is evaluated to determine the interaction of the applied thrust S and the tilt angle μ, resulting in a symmetric shape for $S < 0$ and $S > 0$.

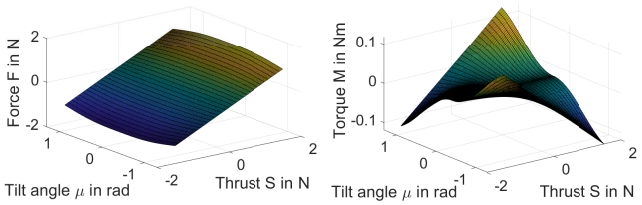

Fig. 2. Actuator characteristics of the traction force $F = \phi_F(S,\mu)$ and the torque $M = \phi_M(S,\mu)$.

The main impacts on these characteristics are the arrangement of the air blades, the diameter of the propeller, and the distance to the center of gravity of the vehicle. For implementing a control strategy for the hovercraft, the required thrust S and tilt angle μ have to be determined to fulfill the desired traction force and torque request. Here, the inverted characteristics

$$S = \phi_S(F,M) \quad \text{and} \quad \mu = \phi_\mu(F,M) \tag{3}$$

are essential. The numerical inversions of both maps are depicted in Fig. 3.

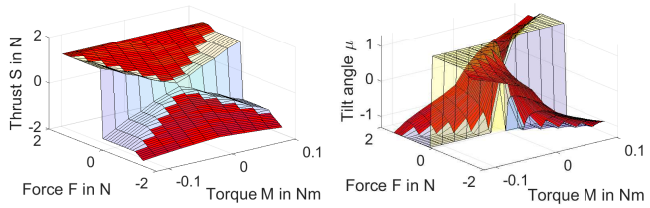

Fig. 3. Inverted actuator characteristics of the propulsion thrust $S = \phi_S(F,M)$ and the tilt angle $\mu = \phi_\mu(F,M)$.

Here, the red colored areas represent applicable operating points, which can be realized with the given traction topology, whereas the transparent parts belong to non-applicable control inputs. To ensure that the control inputs are applicable with the given traction topology, a heuristic correction approach is implemented, which is illustrated in Fig. 4. Here, the valid

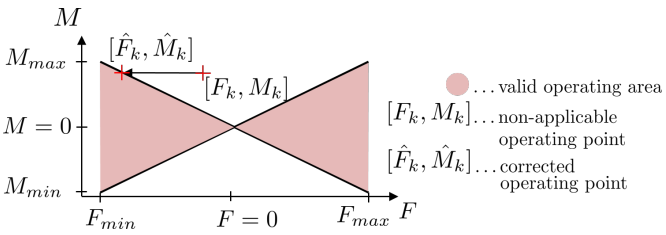

Fig. 4. Correction of non-applicable control inputs considering the inverted actuator characteristic.

operating area is given by

$$M(F) \in [-m_{FM}F\,\mathrm{sign}(F)\ ,\ m_{FM}F\,\mathrm{sign}(F)]\ , \tag{4}$$

with

$$m_{FM} = \frac{M_{max}}{F_{max}} \tag{5}$$

defining the slope of the boundaries, resulting from the maximum force and torque. For a non-applicable pair of control inputs $[F_k,\ M_k]$, the corrected control inputs $[\hat{F}_k,\ \hat{M}_k]$ are determined by increasing the magnitude of the force in order to fulfill the torque request. Hence, the corrected operating point is given by

$$\hat{F}_k = \frac{1}{m_k}M_k \quad \text{and} \quad \hat{M}_k = M_k, \tag{6}$$

with the slope of the exceeded boundary m_k given with

$$m_k = m_{FM}\,\mathrm{sign}(F)\,\mathrm{sign}(M)\ . \tag{7}$$

Considering this restriction, the control inputs are implemented on the hovercraft vehicle as indicated in Fig. 5. The rela-

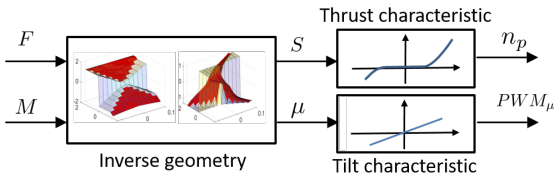

Fig. 5. Implementation of the desired control inputs F and M at the actuators of the vehicle.

tionship between the rotational speed n_p and the resulting thrust S is identified for a neutral position of the air blades, which correspond to a vanishing tilt angle. Fig. 7 shows the characteristic in forward and backward directions. For the control of the motor of the tiltable blades, a linear characteristic is identified that describes the resulting PWM-signal (pulse-width modulation) for the required tilt angle.

III. Trajectory Planing and Optimal Feedforward Control

The main objective of this section is trajectory planning and the derivation of an optimal feedforward control for the horizontal dynamics of the hovercraft vehicle.

In contrast to a non-holonomic vehicle, e.g. a car or a two-wheeled mobile robot, the hovercraft is able to perform lateral movements. Thus, a fully actuated hovercraft is able to perform an evasive maneuver with different driving styles. On the one hand, the vehicle can perform a rotation to change the direction, see Fig. 6 (a). On the other hand, only a lateral movement may be applied to follow the desired trajectory in the $xy-$plane, see Fig. 6 (b). For the existing under-actuated

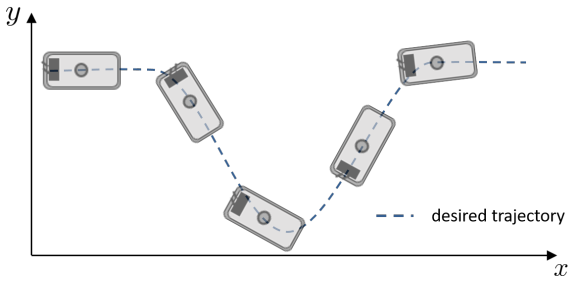

(a) Evasive maneuver based on rotations

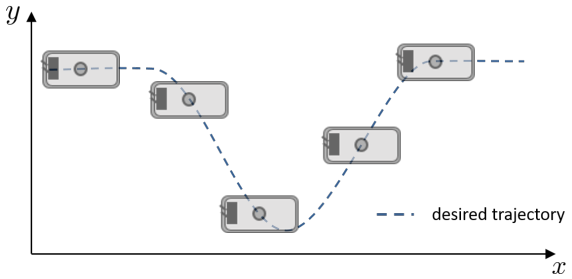

(b) Evasive maneuver based on lateral motions

Fig. 6. Idealized driving styles for an evasive maneuver for a fully actuated hovercraft vehicle.

hovercraft, however, a trade-off between these driving styles becomes necessary, which is characterized by the vehicle dynamics. To determine a feedforward control for the tracking of a desired trajectory of the vehicle in the global xy-plane, the undisturbed state-space representation according to (1) and (2) is given by

$$\underbrace{\begin{bmatrix}\dot{x}\\ \dot{y}\\ \dot{\gamma}\\ \dot{u}\\ \dot{v}\\ \dot{r}\end{bmatrix}}_{\dot{\underline{x}}} = \underbrace{\begin{bmatrix}\cos(\gamma)\cdot u-\sin(\gamma)\cdot v\\ \sin(\gamma)\cdot u+\cos(\gamma)\cdot v\\ r\\ -\frac{d}{m}u+v\cdot r+\frac{1}{m}F\\ -\frac{d}{m}v-u\cdot r\\ -\frac{d_r}{J}r+\frac{1}{J}M\end{bmatrix}}_{\underline{f}(\underline{x},\underline{u},\underline{z})}. \tag{8}$$

Please note that the modeled disturbance forces ΔF and

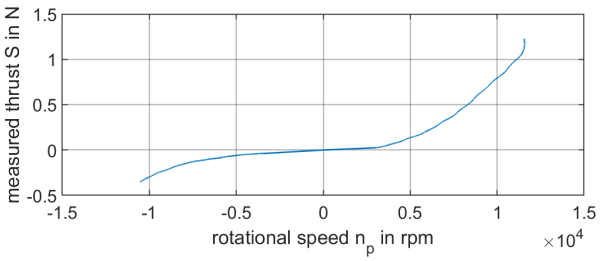

Fig. 7. Identified force characteristic in forward and backward directions.

ΔM are not considered within the feedforward control design. Instead, external disturbances as well as modeling errors are counteracted by feedback control.

For the desired output trajectories $\underline{y}_d(t) = [x_d(t) \;\; y_d(t)]^T$, the optimal control $\underline{u}^*(t) = [F^*(t),\; M^*(t)]^T$ for an evasive maneuver is determined by solving a dynamic optimization optimization problem

$$[F^*(t),\quad M^*(t)] = \arg\left\{\min_{\underline{u}}\{J(\underline{x},\underline{u})\}\right\}, \tag{9}$$
$$\text{s.t. } \dot{\underline{x}} = \underline{f}(\underline{x},\underline{u}),\; \underline{x}(0) = \underline{x}_0,\; \underline{x}(T) = \underline{x}_T,$$

defined by the following finite-time cost functional

$$J = \int_0^T \underbrace{\frac{1}{2}\left[\Delta\underline{y}^T\underline{Q}\Delta\underline{y}+\underline{u}^T\underline{R}\underline{u}\right]}_{f_0}\mathrm{d}t\,. \tag{10}$$

This cost functional contains quadratic terms regarding the output error

$$\Delta\underline{y} = \underline{C}\underline{x}-\underline{y}_d,\quad \text{with}\quad \underline{C} = \begin{bmatrix}1&0&0&0&0&0\\0&1&0&0&0&0\end{bmatrix} \tag{11}$$

and the control inputs $\underline{u}$. Here, the weighting matrices $\underline{Q} = \mathrm{diag}(q_x,q_y) > 0$ and $\underline{R} = \mathrm{diag}(r_F,r_M) > 0$ characterize the desired system behavior. With the integrand f_0 of the cost functional and the given non-linear system model according to (8), the Hamiltonian can be stated as

$$H = -f_0+\underline{p}^T\underline{f}(\underline{x},\underline{u}), \tag{12}$$

where $\underline{p}$ denotes the co-states of the system. The optimal control law in the case without input constraints

$$\underline{u}^* = \underline{R}^{-1}\,\underline{p}^T\left(\frac{\partial \underline{f}(\underline{x},\underline{u})}{\partial \underline{u}}\right) \tag{13}$$

maximizes the given Hamiltonian. Finally, the optimal control is obtained by solving a two-point boundary value problem for the given system of canonical equations

$$\dot{\underline{x}} = \left.\frac{\partial H}{\partial \underline{p}}\right|_{\underline{u}=\underline{u}^*} = \underline{f}\,(\underline{x},\underline{u}^*)\,,\quad \dot{\underline{p}} = -\left.\frac{\partial H}{\partial \underline{x}}\right|_{\underline{u}=\underline{u}^*},$$
$$\underline{x}(0) = \underline{x}_0,\ \underline{x}(T) = \underline{x}_T\ . \tag{14}$$

In Fig. 8, the resulting xy-trajectory is depicted, showing that the desired motion is realized by the determined trajectory. The

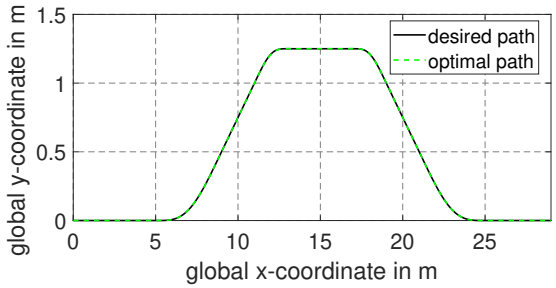

Fig. 8. Optimized vehicle trajectory in the *xy*-plane.

optimal velocities u^*, v^*, r^*, see Fig. 9, and the corresponding control inputs F^*, M^*, see Fig. 10, are presented as well. In Fig. 10, the red phases specify non-applicable operating points. The correction is implemented according to Eq. (6) and is presented in green. Obviously, the implemented increase of the traction force will lead to an occasionally increased longitudinal velocity of the hovercraft – however, this trade-off has to be accepted to fulfill the torque request.
The optimized velocities u^*, v^* and r^* are utilized as desired reference signals for the implementation of the velocity control in Sect. V. Additionally, the optimized control inputs $F^*(t)$ and $M^*(t)$ are implemented as a feedforward control in Sect. V.

IV. Sliding-Mode Control of the Horizontal Vehicle Dynamics

The main objective of this section is the non-linear sliding-mode control (SMC) design for the horizontal dynamics of the hovercraft vehicle. The vertical dynamics corresponds to the description in [2] and is not discussed here. In this paper, sliding-mode techniques are applied to consider the non-linear dynamics of the system in the presence of uncertainty. The robust control approach involves a fast control of the longitudinal velocity, representing the first control output $y_1(t) = u(t)$. The controlled longitudinal velocity is considered subsequently in the robust sliding-mode control of the lateral velocity $y_2 = v(t)$.

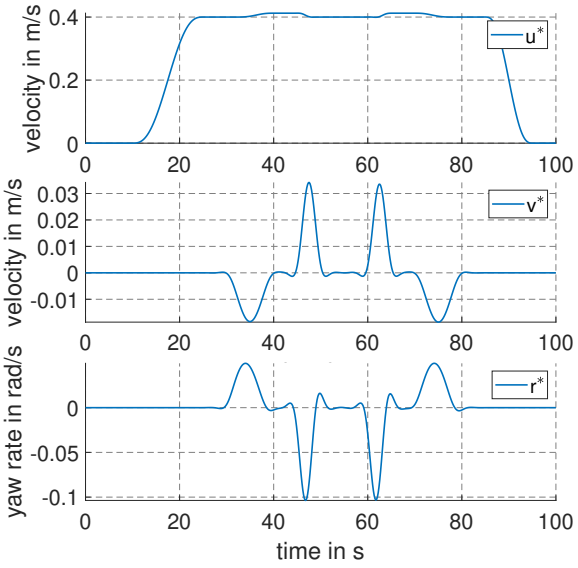

Fig. 9. Body-fixed velocities for the optimized trajectories.

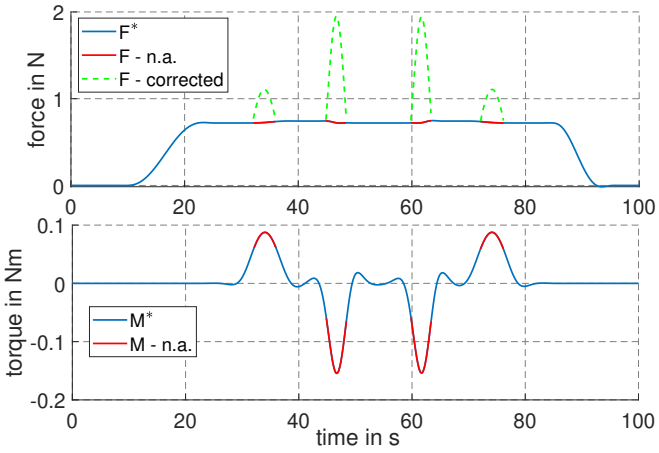

Fig. 10. Optimized control inputs for the given maneuver.

A. Control of the Longitudinal Motion

The control objective w.r.t. the longitudinal motion is minimizing the tracking error $e_u(t) = u_d(t) - u(t)$. Here, the desired speed $u_d(t)$ is determined by the optimal trajectory planning in Sect. III. The resulting error dynamics can be stated with

$$\dot{e}_u(t) = \dot{u}_d(t) - \underbrace{\left(\frac{d}{m}u(t) + v(t)\cdot r(t) - \frac{1}{m}F(t)\right)}_{\dot{u}(t)}. \tag{15}$$

To stabilize this error dynamics, the sliding surface s_u is introduced as the velocity tracking error

$$s_u(t) = e_u(t) = (u_d(t) - u(t))\,. \tag{16}$$

In general, for the sliding-mode approach, the Control Lyapunov function (CLF) $V_u\,(s_u(t)) = \frac{1}{2}s_u^2(t)$ for the scalar sliding

surface $s_u(t)$ has to meet the following sliding condition

$$\dot{V}_u(t) = s_u(t) \cdot \dot{s}_u(t) \leq -\gamma_u \cdot |s_u(t)| = -\gamma_u \cdot s_u(t) \cdot \text{sign}(s_u(t)), \tag{17}$$

where γ_u parametrizes the convergence towards the sliding surface. By introducing $\tilde{\gamma}_u > \gamma_u$, with the sliding surface according to (16) and the error dynamics (15), this requirement can be fulfilled by

$$\dot{u}_d(t) - \left(\frac{d}{m}u(t) + v(t)r(t) - \frac{1}{m}F(t)\right) = -\tilde{\gamma}_u s_u(t) \text{sign}\left(s_u(t)\right). \tag{18}$$

As a result, the control low for the traction force is given by

$$F(t) = m\left(\dot{u}_d(t) + \tilde{\gamma}_u \cdot \text{sign}\left(s_u(t)\right) + \frac{d}{m}u(t) - v(t)r(t)\right). \tag{19}$$

To mitigate chattering effects, a regulation of the unsteady sign-function can be implemented, utilizing the approximation

$$\text{sign}\left(s_u(t)\right) \approx \tanh\left(\frac{s_u(t)}{\varepsilon}\right), \tag{20}$$

with $0 < \varepsilon \ll 1$, which leads to a real sliding mode instead of an ideal one. As it becomes relevant in Sect. V, it is worth pointing out that the control law (19) can be separated in two parts, namely the feedforward part

$$F_{FF}(t) = du(t) - mv(t)r(t), \tag{21}$$

which is based on the inverse dynamics as well as the feedback part

$$F_{FB}(t) = m\left(\dot{u}_d(t) + \tilde{\gamma}_u \cdot \text{sign}\left(s_u(t)\right)\right), \tag{22}$$

according to the desired error dynamics of the controller.

B. Control of the Lateral Motion

In analogy, the dynamics of the lateral velocity tracking error can be stated with $\dot{e}_v(t) = \dot{v}_d(t) - \dot{v}(t)$. Here, the Hurwitz polynomial of the sliding surface

$$s_v(t) = \dot{e}_v(t) + \alpha_v e_v(t) \tag{23}$$

is parametrized by the coefficient α_v. To ensure the negative definiteness of the CLF $V_v(s_v(t)) = \frac{1}{2}s_v^2(t)$, the sliding condition is chosen as

$$\dot{s}_v(t) = \ddot{e}_v(t) + \alpha_v \dot{e}_v(t) \leq -\gamma_v \cdot \text{sign}(s_v(t)). \tag{24}$$

By employing $\tilde{\gamma}_v > \gamma_v$ and with

$$\ddot{e}_v = \ddot{v}_d(t) + \frac{d}{m}\dot{v}(t) + \dot{u}(t)r(t) + u(t)\underbrace{\left(-\frac{d_r}{J}r(t) + \frac{1}{J}M(t)\right)}_{\dot{r}(t)}, \tag{25}$$

(24) can be fulfilled, and the non-linear control law for the torque can be determined in the form

$$M(t) = -\frac{J}{u(t)}\left(\nu_v + r(t)\dot{u}(t) + \frac{d}{m}\dot{v}(t) - \frac{d_r}{J}r(t)u(t)\right). \tag{26}$$

Here, the desired behavior is defined by both a desired linear error dynamics as well as the switching term

$$\nu_v = \ddot{v}_d + \alpha_v\left(\dot{v}_d(t) - \dot{v}(t)\right) + \tilde{\gamma}_v \cdot \text{sign}\left(s_v(t)\right) \ . \tag{27}$$

To avoid the the singularity in (26), the control of the lateral movement is only activated for longitudinal velocities $|u(t)| \geq u_{min}$. Additionally, the control law for the lateral movement (26) also includes the underlying longitudinal velocity control according to (19). This emphasizes that the longitudinal dynamics also effects the control of the lateral movement.
In analogy to (21) and (22), the overall control law for the traction torque can be split as well. By evaluating the inverse dynamics, the feedforward control becomes

$$M_{FF}(t) = -\frac{J}{u(t)}\left(r(t)\dot{u}(t) + \frac{d}{m}\dot{v}(t) - \frac{d_r}{J}r(t)u(t)\right), \tag{28}$$

whereas the feedback part is given by

$$M_{FB}(t) = -\frac{J}{u(t)}\left(\ddot{v}_d + \alpha_v\left(\dot{v}_d(t) - \dot{v}(t)\right) + \gamma_v \cdot \text{sign}\left(s_v(t)\right)\right). \tag{29}$$

V. Performance assessment based on Simulations

This section is dedicated to the investigation of the proposed feedforward and feedback control structure. For the assessment of both quality and practicability of the implemented techniques, several simulations are performed.
For implementing the optimal trajectory from Sect. III as well as the sliding-mode control from Sect. IV, two almost equivalent approaches are depicted in Fig. 11.

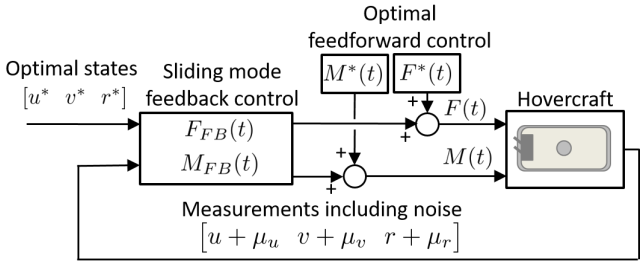

(a) Implementation based on the optimal feedforward control F^* and M^*

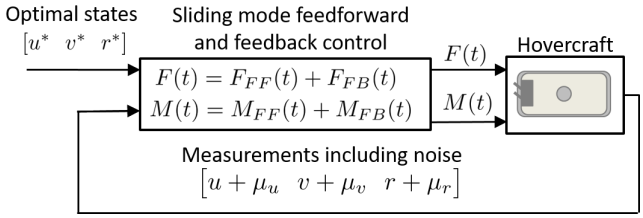

(b) Implementation based on the complete sliding mode approach

Fig. 11. Implementation of the feedforward and feedback control.

The approach presented in Fig. 11 (a) utilizes the determined optimal feedforward control, which directly employs the result of the optimal trajectory planning in Sect. III. Here, only the feedback part of the sliding-mode control law is used. For the second approach according to Fig. 11 (b), the overall

control law is implemented – including both the feedforward part as well as the feedback part. For a realistic simulation of the real hovercraft motion, Gaussian white measurement noise $\underline{\mu}_x = [\mu_u(t) \quad \mu_v(t) \quad \mu_r(t)]^T$ is implemented, interfering the feedback of the body-fixed velocities $\underline{x}_b$. Additionally, an external disturbance force ΔF is considered, see Fig. 12, to assess the capability of the controller to reject external disturbances. The associated simulation results are shown below for the combined feedforward and feedback controller: The velocities are given in Fig. 13, and the corresponding control inputs are depicted in Fig. 14.

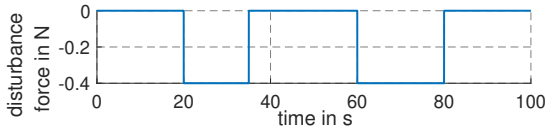

Fig. 12. Additive traction force ΔF as simulated external disturbance.

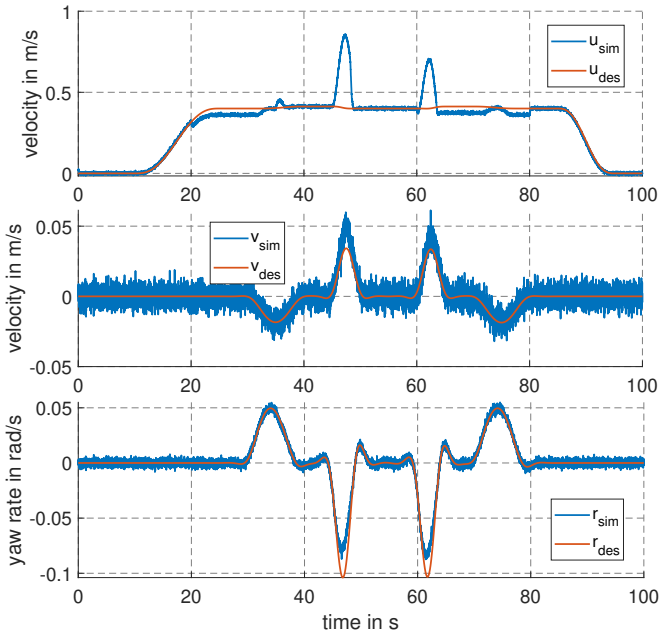

Fig. 13. Simulated body-fixed velocities $[u(t) \quad v(t) \quad r(t)]$ for the sliding-mode control.

As visible in Fig. 13, the desired velocities can be tracked with an acceptable tracking error. The velocity profile of the longitudinal velocity $u(t)$ shows the effect of increasing the applied traction force in order to cope with the inverted actuator characteristics. This effect is also emphasized by the traction force profiles in Fig. 14. Here, the amount of the feedforward control is plotted with a black dotted line, which is extended by the feedback controller – the resulting control input is depicted in blue. Here, the contradictory cross-couplings become obvious: a heuristic shift in the traction force to attain a feasible point in the actuator characteristics causes an decrease of the traction force by the controller to achieve a small tracking error. To avoid this trade-off, a more

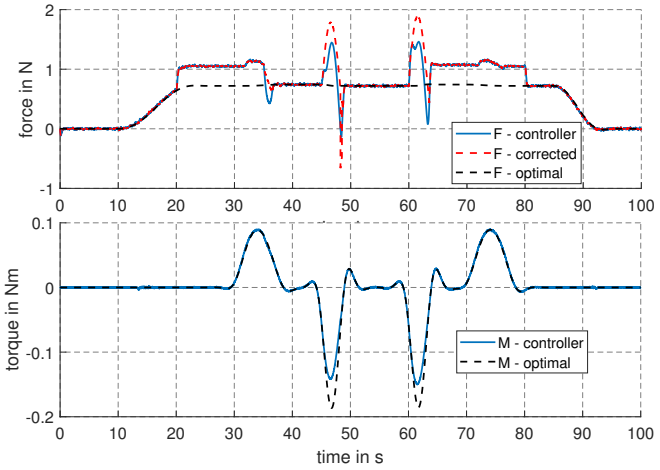

Fig. 14. Simulated control inputs $[F(t) \quad M(t)]$ for the sliding-mode control.

sophisticated trajectory planning approach is necessary that includes the actuator characteristics in the calculation of the optimal reference trajectories.

VI. Conclusions

In this paper, a non-linear velocity tracking control concept for a hovercraft vehicle is presented using body-fixed velocity coordinates. The reference signals are determined by solving a dynamic optimization problem for the trajectory planning in the global coordinate system. By utilizing a proper heuristic to correct non-applicable operating points, the control inputs can be applied in a way that complies with the mechanical restrictions of the traction topology. Taking advantage of sliding-mode techniques, non-linear control laws for the hovercraft are determined that address the system nonlinearities as well as uncertainties properly and realize a desired close-loop tracking error dynamics.

References

[1] T.I. Fossen, Guidance and Control of Ocean Vehicles. Wiley, 1994.

[2] H. Aschemann and A. Rauh, "Nonlinear Control and Disturbance Compensation for Underactuated Ships Using Extended Linearisation Techniques," in *Proc. of the 8th IFAC Conf. on Control Applications in Marine System*, Rostock-Warnemünde, Germany, 2010.

[3] M. Reyhanoglu, "Exponential Stabilization of an Underactuated Autonomous Surface Vessel," in *Automatica*, vol. 33, no. 12, pp. 2249–2254, 1997.

[4] H. Sira-Ramírez and C. A. Ibáñez, "On the Control of the Hovercraft System," in *J. Dynamics and Control*, vol. 10, no. 2, pp. 151–163, 2000.

[5] H. Seguchi and T. Ohtsuka, "Nonlinear Receding Horizon Control of an RC Hovercraft," in *Proc. of the Intern. Conf. on Control Applications*, Glasgow, U.K., pp. 1076-1081 2002.

[6] H. Sira-Ramírez and C. A. Ibáñez, "Dynamic Second-Order Sliding Mode Control of the Hovercraft Vessel," in *IEEE Trans. on Control Systems Techn.*, vol. 10, no. 6, pp. 860–865, 2002.

[7] Lukas Pröhl and Harald Aschemann, "Nonlinear Observer-Based Control of an Under-Actuated Hovercraft Vehicle," in *Proc. of 21th IFAC World Congress*, Berlin, Germany, pp. 8973-8978, 2020.

[8] V. Utkin and H.-C. Chang, "Sliding Mode Control on Electro-Mechanical Systems," in *Mathematical Problems in Engineering*, vol. 8, no. 6, CRC Press, pp. 451–473, 2002.